

# The anti-oxidation behavior and infrared emissivity property of SiC/ZrSiO<sub>4</sub>–SiO<sub>2</sub> coating

Yang Li · Wei Zhou · Peng Xiao · Heng Luo ·  
Zhong-liu Wen · Wei Luo

Received: 30 June 2014 / Accepted: 12 September 2014 / Published online: 26 September 2014  
© Springer Science+Business Media New York 2014

**Abstract** In order to improve the oxidation resistance and decrease the infrared emissivity of carbon/carbon(C/C) composites, the SiC and SiC/ZrSiO<sub>4</sub>–SiO<sub>2</sub> (SZS) coating were prepared by pack cementation and slurry painting method. The phase compositions and microstructures of the as-prepared coatings were characterized by X-ray diffraction, scanning electron microscopy and energy dispersive spectrometer. The anti-oxidation property, failure and infrared emissivity of single SiC coating and SZS coating were investigated. The results show that the weight loss of single SiC coated sample reached  $2.1 \pm 0.025$  % after 58 h isothermal oxidation at 1,500 °C. While the SZS coating exhibits superior oxidation resistance and can protect C/C matrix from oxidation for more than 198 h with a weight-gain of  $3.67 \pm 0.025$  %. The failure mechanisms of single SiC coating are mainly resulting from unself-healing defects caused by the CO<sub>2</sub> gas which generated during the oxidation process of SiC. The investigation of infrared emissivity property reveals that, the infrared emissivity of SZS coating increases gradually from 0.45 to 0.72 between 3 and 14 μm. The infrared emissivity at 500 °C increases gradually from 0.2 to 0.65 between 3 and 14 μm. The coupled effect between dipole moments and lattice vibration in higher temperature becomes weaker, which in turn lead to the reducing of infrared emissivity in turn. From the anti-oxidation and infrared emissivity property point of view, the SZS coating may be one of the most promising candidates for the anti-oxidation at high temperature and low infrared emissivity of C/C composite.

## 1 Introduction

Recently, with the rapid development of electronic devices and electromagnetic wave detection technique, thermal infrared detection had become one of the main means of detection, and thus more and more attention was paid to improve the viability of thermal structures such as missiles using in some harsh environments. For these requirement, the high temperature resistance materials with low-infrared-emissivity are considered as one of the promising solutions [1–4].

Carbon/Carbon (C/C) composites possess many advantages such as light weight, high strength and modulus at high temperature. And they are considered to be the most promising candidate of high-temperature structural materials [5–7]. With the expanding application of C/C composites in thermal structures, the requirement for low infrared emissivity and good oxidation resistance of C/C composites is more and more urgent. However, the infrared emissivity of C/C composites reach up to a relatively high value 0.8 [8], which is easily detected by an infrared detector. Meanwhile, the oxidation of C/C composites above 400 °C limits its application at high temperatures in the oxidizing atmosphere environment [9, 10]. Thus, a great deal studies on curing Achilles' heel of C/C composites have been carried out [11, 12].

The coating technology has considered to be the most reasonable choice to solve these problems well over the years [13, 14]. Silicon carbide (SiC) coating with good physical and chemical compatibility to C/C matrix, was widely used as the bonding layer between C/C and outer ceramic layer to provide well protection for C/C composites, and its infrared emissivity is at a relative low rate when compared with C/C [15–17]. However, the single SiC layer can not provide a long-term protection

Y. Li · W. Zhou · P. Xiao (✉) · H. Luo · Z. Wen · W. Luo  
State Key Laboratory for Powder Metallurgy, Central South University, Changsha 410083, People's Republic of China  
e-mail: xiaopengcsu@csu.edu.cn

for carbon matrix [18–20]. Hence, Great efforts in order to improve the anti-oxidation of C/C composites were to focus on the silicon-based multilayer coatings [17, 18, 21, 22]. Zirconium silicates ( $\text{ZrSiO}_4$ ) has been considered as a candidate materials being applied at high-temperature for its excellent chemical stability, low coefficient of thermal expansion ( $4.1 \times 10^{-6}/^\circ\text{C}$  at  $1,400^\circ\text{C}$ ) and infra-emissivity [23, 24]. In recent years,  $\text{ZrSiO}_4$  coating prepared by the hydrothermal electrophoretic deposition (HTED) or sol–gel method has manifested well performances in oxidation resistance [25–27]. However, none of infra-emissivity studies of these coatings have been reported yet.

In this paper, the SiC bonding layer was prepared by pack cementation. And in order to simplify the preparation process, the  $\text{ZrSiO}_4$ – $\text{SiO}_2$  coating on the SiC coating was prepared by slurry painting technique for its easy operation and relative low cost compared with HTED and sol–gel. The SiC/ $\text{ZrSiO}_4$ – $\text{SiO}_2$  (SZS) coating was expected to protect C/C composite at  $1,500^\circ\text{C}$  for a long time and reduce its infra-emissivity simultaneously. The microstructures, the isothermal anti-oxidation behavior at  $1,500^\circ\text{C}$  and the infra-emissivity at 90 and  $500^\circ\text{C}$  are primarily reported.

## 2 Experimental procedure

### 2.1 Preparation of coatings

The small specimen ( $20 \times 20 \times 5$  mm) as substrates were cut from bulk three-dimensional C/C composites (prepared in Boyun new material Co. Limited, Changsha, China) with a density of  $1.70 \text{ g cm}^{-3}$ . The specimens were polished by SiC abrasive paper and cleaned with ethanol, then followed by drying at  $120^\circ\text{C}$  for 2 h. The pack chemistries for pack cementation included: Si 60–65 wt%, carbon black 5–10 wt%,  $\beta$ -SiC 10–30 wt% and  $\text{Al}_2\text{O}_3$  0–5 wt%. All the powders were analytically graded and mixed together by ball-milling for 2 h. The C/C composites specimens and the powder mixtures were placed in a graphite crucible, and heated to  $1,900^\circ\text{C}$  for 2 h in an argon atmosphere and then held at  $1,900^\circ\text{C}$  for 2 h to form the SiC coating. After the preparation of SiC layer, the  $\text{ZrSiO}_4$ – $\text{SiO}_2$  coating was obtained on the as-prepared SiC coating surface by slurry painting method. The slurry painting chemistries in this procedure included: 20–60 wt%  $\text{SiO}_2$ , 30–60 %  $\text{ZrO}_2$  and 0–5 % sinter aids. All the powders were analytically graded and mixed together by ball-milling with the solution containing 3 wt% polyvinyl alcohol (PVA) for 2 h. After slurry painting process, the coated specimens were dried at  $100^\circ\text{C}$  and then pre-oxidated at  $1,500^\circ\text{C}$  for 1 h to form the  $\text{ZrSiO}_4$ – $\text{SiO}_2$  coating.

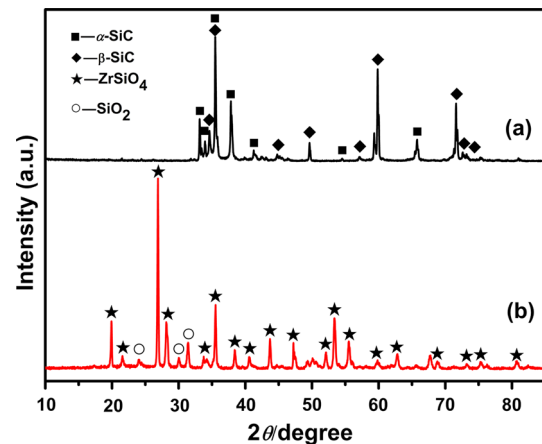


**Fig. 1** The XRD patterns of coatings **a** SiC coating, **b** SZS coatings after pre-oxidation

### 2.2 Testing and characterization

The process of isothermal oxidation test was that the specimens were placed in a mullite crucible and heated at  $1,500^\circ\text{C}$  in ambient air in a tube furnace for a certain of hours. The cumulative weight change percentages ( $\Delta w$ ) of the specimens were described by the following expression and was reported as a function of time:

$$\Delta w = \frac{m_i - m_0}{m_0} \times 100 \% \quad (1)$$

where  $m_0$  and  $m_i$  are measured by electronic balance with sensitivity of  $\pm 0.1$  mg and represents the weight of the specimens before and after oxidation respectively.

The morphology and phase composition of the coatings was investigated by scanning electron microscopy (SEM, Jeol-6300LV) combined with an energy dispersive spectroscopy (EDS) and X-ray diffraction (XRD) analyzer (Rigaku Ltd., Japan, Cu K $\alpha$  radiation).

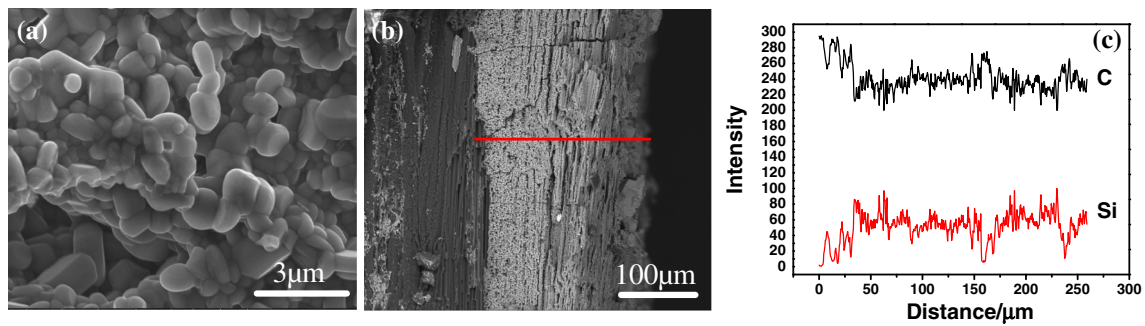
The infra-emissivity of coating at 90 and  $500^\circ\text{C}$  were tested by the InSb/MCT detector.

## 3 Results and discussion

### 3.1 Microstructure of the coating

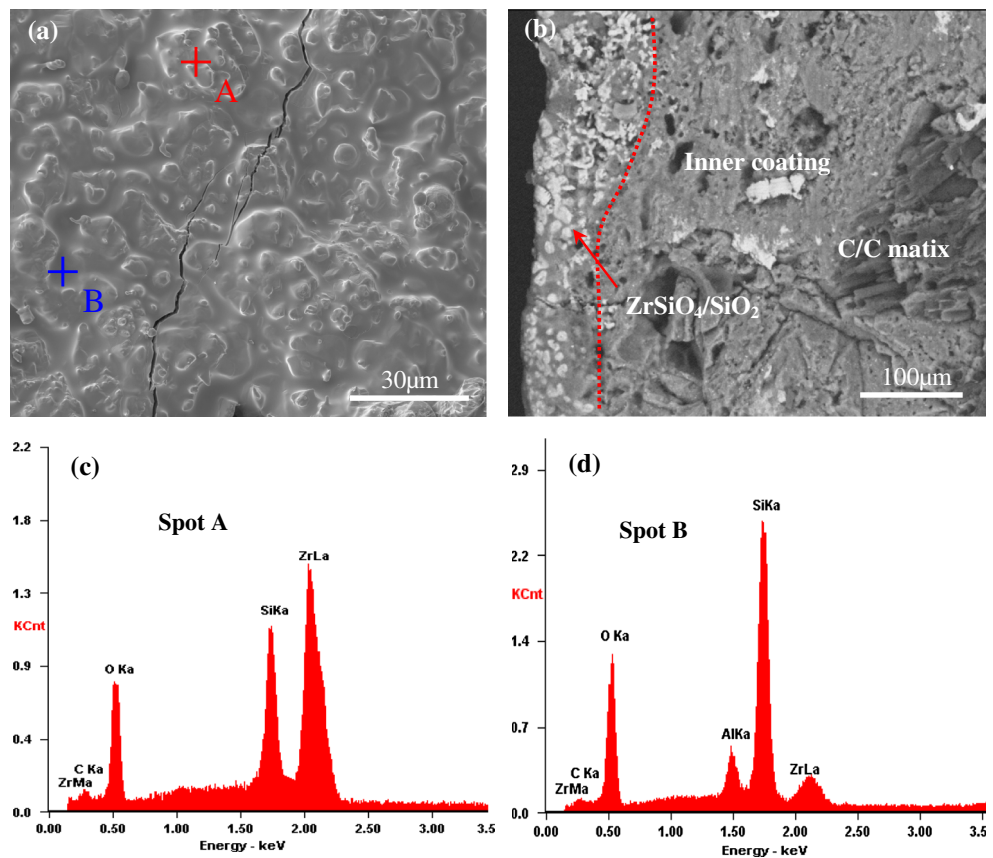
Figure 1 shows the XRD patterns of SiC coating prepared by PC and the SZS coatings after pre-oxidation. As Fig. 1 shown, the SiC coating was mainly composed of  $\alpha$ -SiC and  $\beta$ -SiC. And the prepared SZS coating was mainly composed of  $\text{ZrSiO}_4$  and  $\text{SiO}_2$ .

Figure 2 shows the SEM micrographs of SiC coating surface, cross-section and element line scanning results. As shown in Fig. 2a, the SiC coating was composed of small



**Fig. 2** SEM micrographs and element line scanning results of the SiC coatings **a** surface SEM graph, **b** cross-section SEM graph, **c** element line scanning curves

**Fig. 3** SEM micrographs and element line scanning results of the SZS coatings after pre-oxidation **a** surface SEM graph, **b** cross-section SEM graph, **c** EDS analysis result of Spot A, **d** EDS analysis result of Spot B



dense aggregates which were almost uniform and smaller than 1 µm in diameter. In addition, this coating surface was so fairly rough as to be beneficial for improving the combination between outer coatings and SiC coating. Figure 2b shows the cross-section SEM micrographs of SiC coating. A porous lamellar structure with a thickness of more than 150 µm and many flaws such as cracks and gaps were observed on the side of this SiC coating. Nevertheless, the porous structure could minimize the thermal stress caused by the thermal expansion mismatch at high temperature effectively [16, 24, 28–30]. Figure 2c shows the element

line scanning results of the SiC coating. The Si and C contents were basically stable in the main body of the SiC coating. Correspondingly, the Si content was growing increasingly from C/C matrix to the outside, while the C content decreased gradually. It suggests that the gradient composition of SiC coating was beneficial to reduce the difference of thermal expansion coefficient between the coating and the matrix [31].

Figure 3 shows the SEM micrographs and element line scanning results of the SZS coatings after pre-oxidation. As shown in Fig. 3a, a dense coating with a few cracks caused

**Table 1** The weight ratio of elements in different area and main materials relating to the spots in Fig. 3

Element	Spot A	Spot B
O	33.73	40.66
Si	11.57	25.56
C	09.84	07.00
Zr	44.86	0.517
Main materials	ZrSiO <sub>4</sub>	SiO <sub>2</sub>

by thermal stress was observed. And the SZS coating surface was composed of bump particles and glass phase. In addition, the Fig. 3c, d show the spot EDS analysis result of Spot A and Spot B marked in Fig. 3a. Furthermore, the elements and their weight ratios of different shaped crystal were summarized in Table 1.

After synthesis analysis of these data, the bump particles in Fig. 3a were mainly composed of ZrSiO<sub>4</sub>, and the glass phase was SiO<sub>2</sub>. The element Al in Table 1 may be imported from the mullite crucible during oxidation at 1,500 °C. Figure 3b shows the cross-section SEM graph of the SZS coatings after pre-oxidation. The thickness of coating was about 200 μm. And the bonding between inner and outer coating was in a pretty well condition. Moreover, the dense ZrSiO<sub>4</sub>-SiO<sub>2</sub> coating presented as a mosaic structure that ZrSiO<sub>4</sub> was embedded into SiO<sub>2</sub>, and this structure is conducive to relieve thermal stress caused by the diversity of CTE (coefficient of thermal expansion) between ZrSiO<sub>4</sub> and SiO<sub>2</sub> coatings, and effectively pin the glass phase to avoid the gasification of SiO<sub>2</sub> and the generation of diffusing defects for oxygen [32].

### 3.2 Anti-oxidation properties

Figure 4 displays the isothermal oxidation curves of SiC and SZS coated C/C composites in ambient air at 1,500 °C. The mass loss were calculated by using formula (1).

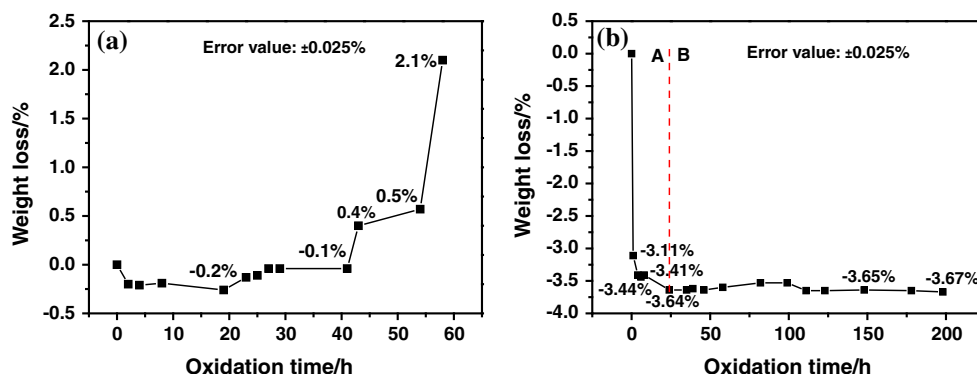
The weight variations of C/C-SiC and SZS coated C/C composites are due to the weight-loss from oxidation of carbon and the weight-gain mainly attributed the oxidation of SiC.

As Fig. 4a shown, the SiC coated sample gain weight quickly within the first 2 h owing to the transformation of SiC into SiO<sub>2</sub>. During the 2–41 h, the weight almost remained stable that weight-loss and the weight-gain were keeping in a balance. However, the weight began to decrease after 41 h oxidation, and the weight-loss reached 0.5 ± 0.025 % at 55th hour. After 58 h oxidation, the weight-loss of coated sample reached 2.1 ± 0.025 %, and finally the coating failed.

Figure 4b shows the isothermal oxidation curves of SZS coated C/C composites in ambient air at 1,500 °C. The oxidation of SZS coated C/C composites can be divided into two processes marked as A and B. Within 24 h (process A), the sample got a rapid weight-gain. And from the 24 to 198 h (process B), the weight of sample remained almost stable, which indicated that the coating displayed good oxidation resistance in ambient air at 1,500 °C. In addition, the quick weight gaining during the pre-oxidation indicated the formation of a mass of SiO<sub>2</sub>. While after the pre-oxidation, the rate of weight-gain decreased due to the self-healing of SiO<sub>2</sub> which slacken the diffusion of O.

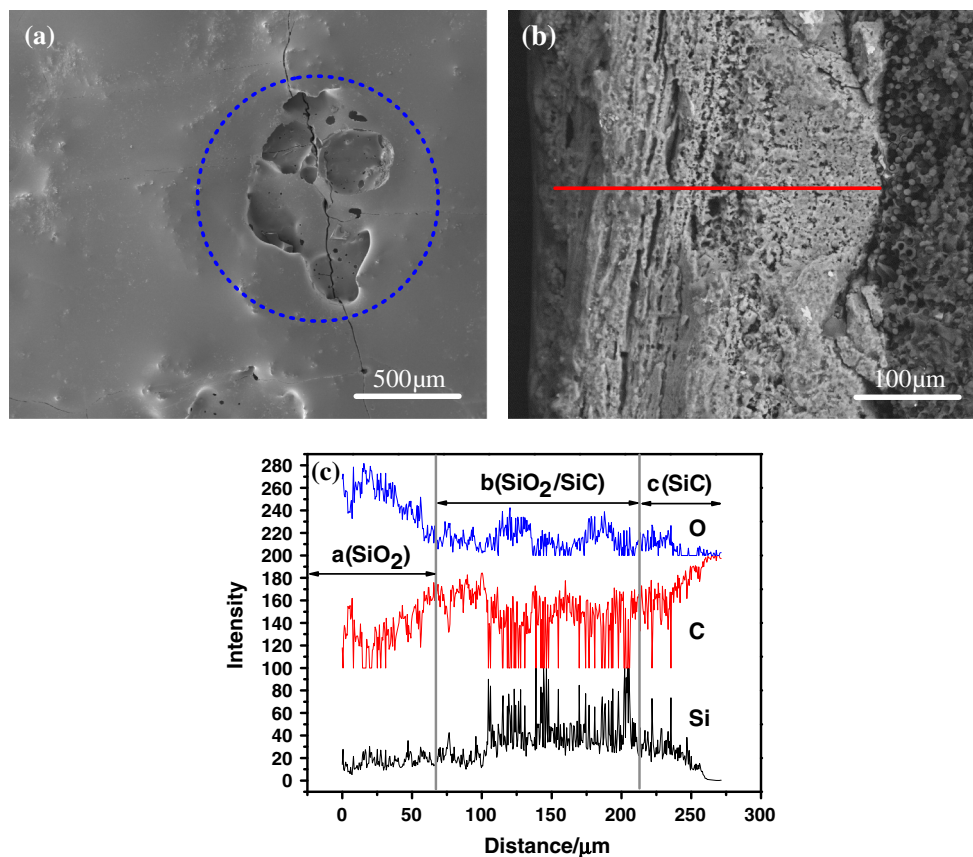
In brief conclusion, the SZS coating shows a pretty well anti-oxidation performance.

Figure 5 shows the surface, cross-section SEM micrographs and element line scanning curves of SiC coating after 58 h oxidation in ambient air at 1,500 °C. Compared with the rough surface before oxidation as shown in Fig. 2, the coating surface shown in Fig. 5a became very dense due to the formation of SiO<sub>2</sub> which could seal the defects and effectively decrease the diffusion velocity of oxygen [17, 33, 34]. Meanwhile, the micro-cracks were also observed in the surface for rapid cooling of sample from 1,500 °C to room temperature. These cracks will be healed



**Fig. 4** The isothermal oxidation curve of the SiC and SZS coated C/C composites in ambient air at 1,500 °C **a** the oxidation curve of the SiC coated C/C composites, **b** the oxidation curve of SZS coated C/C composites

**Fig. 5** The surface, cross-section SEM micrographs and element line scanning curves of SiC coatings after 58 h oxidation in ambient air at 1,500 °C **a** surface SEM graph, **b** cross-section SEM graph, **c** element line scanning curves



gradually at high temperature and almost have no detrimental effect. Whereas the pores on the coating surface as shown in the cycled area of Fig. 5a were generated after the breakage of CO<sub>2</sub> air bubble caused by the oxidation of C. The pores can not self-healed quickly for the limited liquidity of SiO<sub>2</sub>, and then promote the diffusion of oxygen [24, 25, 35, 36].

As Fig. 5b shown, compared with the porous loose structure before oxidation as shown in Fig. 2, the coating experienced 58 h oxidation had became rather dense. Meanwhile, some regular pores which may store the CO<sub>2</sub> during the oxidation process were observed from the areas of matrix to surface. And these pores were beneficial for the diffusion of oxygen [16].

Figure 5c displays the cross section EDS line scanning analyses of the SiC coating after 58 h oxidation in ambient air at 1,500 °C. The EDS Line scanning analyses of O, C and Si elements show that the coating can be divided into three parts, designated as part a, b and c as shown in Fig. 5c. In part a, it had a higher O content than the others two parts, and the coating in this part was mainly comprised of SiO<sub>2</sub>. In part b, the C and O contents remained balanced owing to the low oxygen diffusion rate of SiO<sub>2</sub>, and the coating in this part was mainly composed of SiC

and SiO<sub>2</sub> phases. In part c, it had a highest C content, and the main composition in this area was SiC.

Taken together, the SiC coating during the oxidation was not completely oxidized into SiO<sub>2</sub> scale until it failed. The SiO<sub>2</sub> scale over the residual SiC coating makes it difficult for the CO<sub>2</sub> gas produced in the oxidation process of SiO<sub>2</sub>/SiC interface and SiC/C interface to diffuse out, which cause the increase of gas pressure and then form air bubbles to separate the dense SiO<sub>2</sub> scale. The defects such as large pores shown in Fig. 5a that air bubble left behind can't healed it quickly by the molten SiO<sub>2</sub> and then promote the diffusion of oxygen. And so, to some extent, the dual-layer coating can solve this problem effectively.

Figure 6 shows the surface and cross-section image of SZS coated sample after oxidation for different times in ambient air at 1,500 °C. According to the Fig. 6a–c, the outer coating surface after oxidation was pretty dense without any large pores caused by breakage of CO<sub>2</sub> air bubbles.

Figure 6d–f show the cross-section SEM micrographs of SZS coating after 4, 46 and 198 h oxidation. From Fig. 6d, e, it can be found that the inner-outer coating and the matrix-inner coating were in a fairly good combination, meanwhile the coatings was relatively dense without large

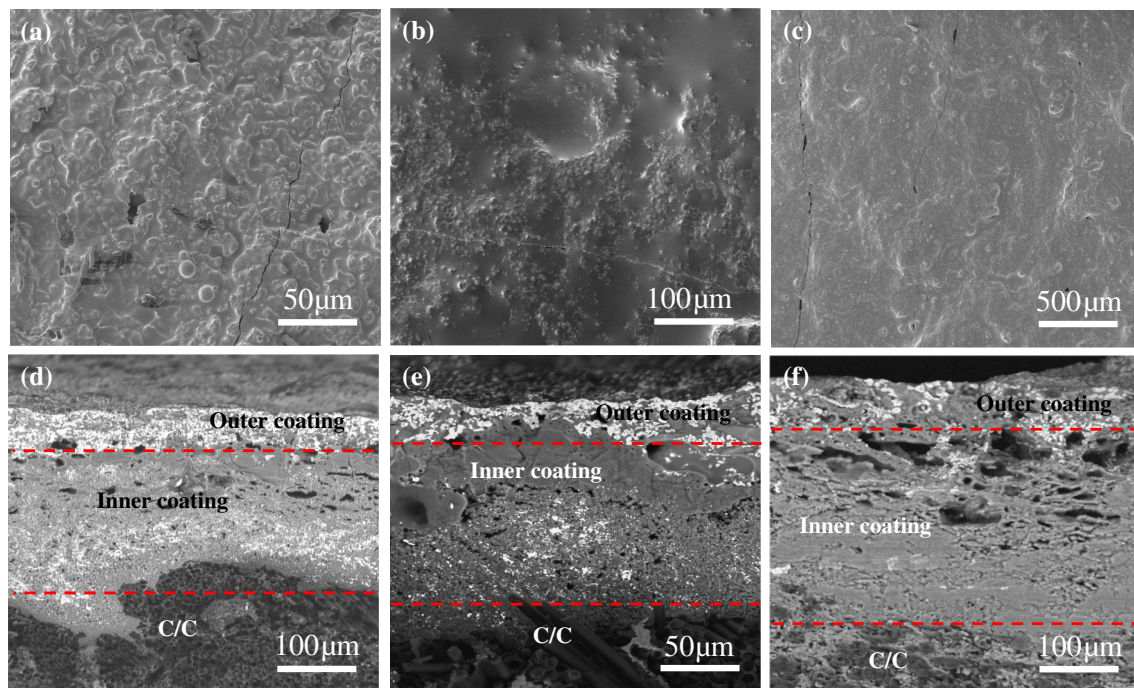


**Fig. 6** The surface and cross-section image of SZS coated sample after oxidation for different times in ambient air at 1,500 °C (a, d 4 h, b, e 46 h, c, f 198 h, a–c surface SEM micrographs, d–f cross-section SEM micrographs)

pores. However, the combination of inner and outer coating after 198 h oxidation was in rather bad condition as a great quantity of holes were found in the interface bonding area as shown in Fig. 6f. And the dense outer coating prevented the CO<sub>2</sub> air to spread outward quickly. The CO<sub>2</sub> air bubbles caused by the oxidation of SiC coating were stored at the interface bonding areas and then the holes formed when the sample were cut at room temperature. The outer coating was heterogeneous including solid ZrSiO<sub>4</sub> and glassy SiO<sub>2</sub>, and went against to the growth of the air bubbles. So the CO<sub>2</sub> air can only spread through the micro-faults such as micro-cracks and micro-pores or the melt SiO<sub>2</sub> of the outer coating and the tiny holes can be healed by the SiO<sub>2</sub> rapidly. In brief, the outer-coating prevented the growing up of air bubbles effectively so there were no large pores in the coating surface as the single SiC coating.

### 3.3 The infrared emissivity of ZrSiO<sub>4</sub>–SiO<sub>2</sub>/SiC coating

Nowadays, as one of the primary means of detecting, the thermal infrared surveillance was mainly focus on 3–5 and 8–14 μm wavebands [37, 38]. Thus a great attention was paid to the infrared emissivity of coating within aforementioned wavebands. The lower infrared emittance means greater survivable ability of objects.

Figure 7 was the infrared emissivity of SiC coating (at 90 °C) and SZS coating (at 90 and 500 °C). As Fig. 7

shown, the infrared emissivity curves of single SiC coated sample at 90 °C were lower than 0.65 and increased gradually from 0.45 to 0.6 within the wavelength range of 3–5 μm, and decreased rapidly from 0.6 to 0.2 between 5 and 12.2 μm wavelength, then drastically increased to 0.6 at 14 μm wavelength. In response to these circumstances, it was related to the absorption of SiC. Notably, the relationship between infrared absorptivity  $\alpha$ , infrared transmittance  $\tau$ , infrared reflectivity  $\rho$  and infrared emissivity  $\varepsilon$  was shown in the Eqs. (2), (3), (4), and (5) as follows:

$$1 = \alpha + \rho + \tau \quad (2)$$

where  $\tau$  is almost equal to 0,

$$1 - \rho = \alpha \quad (3)$$

Then

$$\alpha = \varepsilon \quad (4)$$

It means

$$\varepsilon = 1 - \rho \quad (5)$$

The infrared wave absorption peak of SiC coating at 12.2 μm, which is consistent with the values reported by previous literature [39], may mainly caused by the electronic transition and lattice vibrations. On one hand, the frequency mismatch of SiC lattice vibration and infrared wave weakened the vibration mode of coupling effect between phonon and photon. On the other hand, the lattice

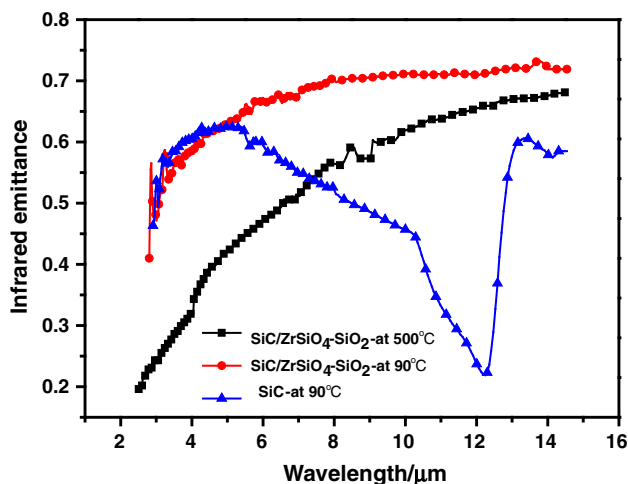


**Fig. 7** The infrared emissivity of SiC coating (at 90 °C) and SZS coating (at 90 and 500 °C)

vibrations weakened the change of dipole moment which, in turn, lowered absorption of infrared wave [39, 40]. This means that there is stronger reflection, lower absorption and lower infrared emissivity within the wavelength range of 10–14 μm.

While coated by SZS coating, the infrared emissivity of sample at 90 °C almost remained almost unchanged as single SiC coated sample between 3 and 5 μm wavelength and increased gradually from 0.68 to 0.72 between 5 and 14 μm. Furthermore, the infrared wave reflection peak disappeared. This was due to the oxidation of SiC into SiO<sub>2</sub> during the pre-oxidation process. Additionally, the infrared emissivity of the whole coating was also affected by the outer ZrSiO<sub>4</sub>-SiO<sub>2</sub> coating.

Compared with SZS coating at 90 °C, as shown in Fig. 7, the infrared emissivity at 500 °C was obvious lower and increased gradually from 0.2 to 0.65 between 3 and 14 μm according to the rising tendency of at 90 °C. Within 3–5 μm wavebands this coating was lower than 0.4, and its low infrared emissivity was beneficial to hide under the detection of infrared detector. While at 8–14 μm, the coating at 500 °C without characteristics reflection of infrared wave was comparatively higher than SiC coating but lower than 90 °C. According to the fundamental infrared physics laws, the higher temperature of an object means lower IR emissivity. According to the Stefan-Boltzmann equation and the law of conservation of energy, the infrared emissivity of object was related to the temperature, and its relevance was shown as Eq. (6) [41, 42]:

$$\epsilon_1 = \frac{(4T^3 + 2\alpha T^4)\epsilon}{T_1^3 + T_1^2 T + T_1 T^2 + T^3 + 2\alpha T^4} \tag{6}$$

The  $\epsilon_1$  at  $T_1$  can be deduced by the  $\epsilon$  at a certain temperature  $T$  and coefficient of linear expansion  $\alpha$

through this equation. While  $T_1 > T$ ,  $\alpha$  was merely in the orders of magnitude which was lower than  $10^{-4}$  but greater than 0, then  $\epsilon_1 < \epsilon$ . It indicates that with higher temperature, the infrared emissivity will be lower. This phenomenon can be explained by the fact that the influence of lattice vibration on infrared wave. The higher the temperature of an object, the higher the lattice vibration frequency. Thus, the coupled effect between dipole moments becomes weaker, which lead to the reducing of infrared wave absorption.

### 4 Conclusion

An anti-oxidation and low infrared emissivity SZS coating for C/C composites were successfully prepared by pack cementation with a later slurry painting. Compared to the  $2.1 \pm 0.025$  % weight-loss of Single SiC coating for 58 h, the as-prepared SZS coating can effectively protect the C/C matrix from oxidation in the air at 1,500 °C for 198 h with a mass gain of  $3.67 \pm 0.025$  %. The reason for the failure of SiC coating was that the breakage of large bubbles caused by the gas generated from oxidation of C element created the high-diffusivity path of oxygen. The SZS coating can effectively prevent these air bubbles from rising up. The infrared emissivity of SZS coating increases gradually from 0.45 to 0.72 between 3 and 14 μm, and the infrared wave reflection peak disappeared compared with SiC coating. The infrared emissivity at 500 °C was obviously lower and increased gradually from 0.2 to 0.65 between 3 and 14 compared with at 90 °C. From the anti-oxidation and infrared emissivity property point of view, the SZS coating may be one of the most promising candidates for the oxidation at high temperature and low infrared emissivity of C/C composite.

**Acknowledgments** The project was supported by the National Key Basic Research and Development Program under Grant No. 2011CB605804 and the National Natural Science Foundation of China under Grant No. 51205417.

### References

1. R. Liu, C. Ji, J.J. Mock, J.Y. Chin, T.J. Cui, D.R. Smith, Broadband ground-plane cloak. *Science* **323**(5912), 366–369 (2009)
2. S.P. Mahulikar, A.G. Rao, P.S. Kolhe, Infrared signatures of low-flying aircraft and their rear fuselage skin’s emissivity optimization. *J. Aircr.* **43**(1), 226–232 (2006)
3. S.P. Mahulikar, H.R. Sonawane, G. Arvind Rao, Infrared signature studies of aerospace vehicles. *Prog. Aerosp. Sci.* **43**(7–8), 218–245 (2007)
4. K.J. Vinoy, *Radar Absorbing Materials: From Theory to Design and Characterization* (Kluwer, Norwell Boston, 1996)
5. N.P. Bansal, *Handbook of ceramic composites* (Springer, Berlin, 2005)

6. K.-Z. Li, X.-T. Shen, H.-J. Li, S.-Y. Zhang, T. Feng, L.-L. Zhang, Ablation of the carbon/carbon composite nozzle-throats in a small solid rocket motor. *Carbon* **49**(4), 1208–1215 (2011)
7. L.-N. Peng, G.-Q. He, J. Li, L. Wang, F. Qin, Effect of combustion gas mass flow rate on carbon/carbon composite nozzle ablation in a solid rocket motor. *Carbon* **50**(4), 1554–1562 (2012)
8. B. Zhu, M. Jing, Study on spectral emissivity of C/C composites. *Spectrosc. Spectr. Anal.* **29**(11), 2909–2913 (2009). (in Chinese)
9. H. Li, D. Yao, Q. Fu, L. Liu, Y. Zhang, X. Yao, Y. Wang, H. Li, Anti-oxidation and ablation properties of carbon/carbon composites infiltrated by hafnium boride. *Carbon* **52**, 418–426 (2013)
10. M.M. Schwartz, *Handbook of structural ceramics* (McGraw-Hill, New York, 1992)
11. H.-J. Li, T. Feng, Q.-G. Fu, H. Wu, X.-T. Shen, Oxidation and erosion resistance of MoSi<sub>2</sub>-CrSi<sub>2</sub>-Si/SiC coated C/C composites in static and aerodynamic oxidation environment. *Carbon* **48**(5), 1636–1642 (2010)
12. H. Zhou, L. Gao, Z. Wang, S. Dong, ZrB<sub>2</sub>-SiC oxidation protective coating on C/C composites prepared by vapor silicon infiltration process. *J. Am. Ceram. Soc.* **93**(4), 915–919 (2010)
13. J.-F. Huang, W. Hao, L.-Y. Cao, L.-X. Yin, H. Ouyang, C.-Y. Yao, J.-P. Wu, J. Fei, An AlPO<sub>4</sub>/SiC coating prepared by pulse arc discharge deposition for oxidation protection of carbon/carbon composites. *Corros. Sci.* **79**, 192–197 (2014)
14. K.-T. Wang, L.-Y. Cao, J.-F. Huang, J. Fei, A mullite/SiC oxidation protective coating for carbon/carbon composites. *J. Eur. Ceram. Soc.* **33**(1), 191–198 (2013)
15. H. Jafari, N. Ehsani, S.A. Khalifeh-Soltani, M. Jalaly, Nano-SiC/SiC anti-oxidant coating on the surface of graphite. *Appl. Surf. Sci.* **264**, 128–132 (2013)
16. H. Jian-Feng, Z. Xie-Rong, L. He-Jun, X. Xin-Bo, F. Ye-wei, Influence of the preparation temperature on the phase, microstructure and anti-oxidation property of a SiC coating for C/C composites. *Carbon* **42**(8–9), 1517–1521 (2004)
17. K.-D. Xia, C.-X. Lu, Y. Yang, Preparation of an anti-oxidative SiC/SiO<sub>2</sub> coating on carbon fibers by a sol-gel method. *Carbon* **63**, 594 (2013)
18. H. Jian-Feng, L. He-Jun, Z. Xie-Rong, L. Ke-Zhi, X. Xin-Bo, H. Min, Z. Xiu-Lian, L. Ying-Lou, A new SiC/yttrium silicate/glass multi-layer oxidation protective coating for carbon/carbon composites. *Carbon* **42**(11), 2356–2359 (2004)
19. Y.-L. Zhang, H.-J. Li, Z.-X. Hu, J.-C. Ren, K.-Z. Li, Microstructure and oxidation resistance of Si-Mo-B coating for C/SiC coated carbon/carbon composites. *Corros. Sci.* **72**, 150–155 (2013)
20. X. Qiang, H. Li, Y. Zhang, Q. Fu, J. Wei, S. Tian, A modified dual-layer SiC oxidation protective coating for carbon/carbon composites prepared by one-step pack cementation. *Corros. Sci.* **53**(1), 523–527 (2011)
21. T. Li, H. Li, X. Shi, Effect of LaB<sub>6</sub> on the thermal shock property of MoSi<sub>2</sub>-SiC coating for carbon/carbon composites. *Appl. Surf. Sci.* **264**, 88–93 (2013)
22. X.-Y. Yao, H.-J. Li, Y.-L. Zhang, J.-J. Ren, D.-J. Yao, J. Tao, A SiC/ZrB<sub>2</sub>-SiC/SiC oxidation resistance multilayer coating for carbon/carbon composites. *Corros. Sci.* **57**, 148–153 (2012)
23. A. Kaiser, M. Lobert, R. Telle, Thermal stability of zircon (ZrSiO<sub>4</sub>). *J. Eur. Ceram. Soc.* **28**(11), 2199–2211 (2008)
24. L. He-Jun, F. Qian-Gang, L. Ke-Zhi, SiC-Si-ZrSiO<sub>4</sub> multiphase oxidation protective coating for carbon/carbon composites. *J. Mater. Sci. Technol.* **24**(06), 941–944 (2009)
25. J. Liu, L.-Y. Cao, J.-F. Huang, Y. Xin, W.-D. Yang, J. Fei, C.-Y. Yao, A ZrSiO<sub>4</sub>/SiC oxidation protective coating for carbon/carbon composites. *Surf. Coat. Technol.* **206**(14), 3270–3274 (2012)
26. J. Liu, J.F. Huang, L.Y. Cao, Y. Xin, ZrSiO<sub>4</sub>/SiC oxidation protective coating for carbon/carbon composites prepared by hydrothermal electrophoretic deposition. *Key Eng. Mater.* **512**, 1070–1073 (2012)
27. C. Sun, H.-J. Li, Q.-G. Fu, H.-L. Li, Y.-J. Wang, H. Wu, ZrSiO<sub>4</sub> oxidation protective coating for SiC-coated carbon/carbon composites prepared by supersonic plasma spraying. *J. Therm. Spray Techn.* **22**(4), 525–530 (2013)
28. Q. Zhu, X. Qiu, C. Ma, Oxidation resistant SiC coating for graphite materials. *Carbon* **37**(9), 1475–1484 (1999)
29. Y.-L. Zhang, H.-J. Li, X.-F. Qiang, K.-Z. Li, S.-Y. Zhang, C/SiC/MoSi<sub>2</sub>-Si multilayer coatings for carbon/carbon composites for protection against oxidation. *Corros. Sci.* **53**(11), 3840–3844 (2011)
30. Y. Chu, H. Li, L. Li, L. Qi, Oxidation protection of C/C composites by ultra long SiC nanowire-reinforced SiC-Si coating. *Corros. Sci.* **84**, 204–208 (2014)
31. Y.-L. Zhang, H.-J. Li, Q.-G. Fu, K.-Z. Li, J. Wei, P.-Y. Wang, A C/SiC gradient oxidation protective coating for carbon/carbon composites. *Surf. Coat. Technol.* **201**(6), 3491–3495 (2006)
32. Y. Zeng, X. Xiong, S. Guo, W.-Z. Zhang, SiC/SiC-YAG-YSZ oxidation protective coatings for carbon/carbon composites. *Corros. Sci.* **70**, 68–73 (2013)
33. O.-S. Kwon, S.-H. Hong, H. Kim, The improvement in oxidation resistance of carbon by a graded SiC/SiO<sub>2</sub> coating. *J. Eur. Ceram. Soc.* **23**(16), 3119–3124 (2003)
34. K. Xia, C. Lu, Y. Yang, Preparation of anti-oxidative SiC/SiO<sub>2</sub> coating on carbon fibers from vinyltriethoxysilane by sol-gel method. *Appl. Surf. Sci.* **265**, 603–609 (2013)
35. N.S. Jacobson, D.J. Roth, R.W. Rauser, J.D. Cawley, D.M. Curry, Oxidation through coating cracks of SiC-protected carbon/carbon. *Surf. Coat. Technol.* **203**(3), 372–383 (2008)
36. K.-T. Wang, L.-Y. Cao, J.-F. Huang, J. Fei, A mullite/SiC oxidation protective coating for carbon/carbon composites. *J. Eur. Ceram. Soc.* **33**(1), 191–198 (2013)
37. L. Chen, C. Lu, Z. Fang, Y. Lu, Y. Ni, Z. Xu, Infrared emissivity and microwave absorption property of Sm<sub>0.5</sub>Sr<sub>0.5</sub>CoO<sub>3</sub> perovskites decorated with carbon nanotubes. *Mater. Lett.* **93**, 308–311 (2013)
38. L.-S. Fu, J.-T. Jiang, L. Zhen, W.-Z. Shao, FeNi<sub>3</sub>/indium tin oxide (ITO) composite nanoparticles with excellent microwave absorption performance and low infrared emissivity. *Mat. Sci. Eng. B* **178**(4), 225–230 (2013)
39. M.E. Thomas, S.K. Andersson, Infrared properties of CVD β-SiC. *Infrared Phys. Technol.* **39**(4), 223–234 (1998)
40. Y.M. Wang, H. Tian, X.E. Shen, L. Wen, J.H. Ouyang, Y. Zhou, D.C. Jia, L.X. Guo, An elevated temperature infrared emissivity ceramic coating formed on 2024 aluminium alloy by microarc oxidation. *Ceram. Int.* **39**(3), 2869–2875 (2013)
41. G. Neuer, G. Jaroma-Weiland, Spectral and total emissivity of high-temperature materials. *Int. J. Thermophys.* **19**(3), 917–929 (1998)
42. D. Alfano, L. Scatteia, S. Cantoni, M. Balat-Pichelin, Emissivity and catalytic measurements on SiC-coated carbon fibre reinforced silicon carbide composite. *J. Eur. Ceram. Soc.* **29**(10), 2045–2051 (2009)